



© 2025. The Author(s). This is an open-access article distributed under the terms of the Creative Commons Attribution-ShareAlike 4.0 International Public License (CC BY SA 4.0, <https://creativecommons.org/licenses/by-sa/4.0/legalcode>), which permits use, distribution, and reproduction in any medium, provided that the article is properly cited.

Effect of humic acid on the adsorption of selenium by lepidocrocite

Shengmao Zhao¹, Jian Zhu*¹, Elias Niyuhire², Ruyi Zheng¹, Wenjian Mao³

¹College of Resource and Environmental Engineering, Key Laboratory of Karst Georesource and Environment, Ministry of Education, Guizhou University, Guiyang 550025, PR China

²Ecole Normale Supérieure, Département des Sciences Naturelles, Centre de Recherche en Sciences et de Perfectionnement Professionnel, Boulevard Mwezi Gisabo, B.P.: 6983 Bujumbura, Burundi

³Guizhou Lvxing Qingyuan Environmental Protection Co., Ltd., Guiyang 550002, PR China

* Corresponding author's e-mail: jzhu@gzu.edu.cn

Keywords: Humic acid; Lepidocrocite; Selenium; Adsorption

Abstract: Selenium (Se) mobility and bioavailability in natural environments are influenced by its adsorption at the aqueous interface of lepidocrocite (Lep), which is significantly affected by humic acid (HA), a common natural organic matter (NOM). This study investigated the mechanisms by which HA influences Se adsorption on Lep, aiming to understand how HA affects Se speciation, distribution, and mobility in natural environments. Batch experiments were conducted using synthetic Lep and HA under varying pH values (4–8) and HA concentrations (10–100 mg C/L). Interactions among HA, Lep, and Se were characterized using Fourier-transform infrared spectroscopy (FTIR) and scanning electron microscopy (SEM). Zeta potential and hydrodynamic diameter measurements were also performed to evaluate colloidal stability. HA significantly reduced Se adsorption on Lep by competing for adsorption sites, forming coordination bonds with Se, and altering Lep's surface charge and hydrophobicity. At higher HA concentrations, dissolved and colloidal Se increased, while particulate Se decreased. Lower pH enhanced Se adsorption due to protonation, whereas higher pH promoted Se mobility. FTIR and SEM analyses confirmed HA's role in modifying Lep's surface properties and influencing Se adsorption behavior. HA plays a critical role in modulating Se adsorption on Lep through competitive adsorption, coordination interactions, and surface modification. These mechanisms influence Se speciation, distribution, and mobility, with implications for managing Se bioavailability in agricultural and environmental systems. This study provides insights into the geochemical cycling of Se and offers guidance for optimizing Se-rich agricultural practices.

Introduction

Selenium (Se) is an essential trace element that performs critical biological functions in the human body. Se deficiency has been linked to various health issues, including cataracts, cardiomyopathy, immune dysfunction, and cognitive decline. It was estimated that over 15% of the global population is affected by Se deficiency (Ying and Zhang 2019). Dietary intake is the primary determinant of Se levels in the body, with food Se content influenced by the concentration and chemical speciation of Se in soil (Li et al. 2017). In natural systems, Se is found in four primary oxidation states: Se(0), Se(-II), Se(IV), and Se(VI) (Ros et al. 2016). Among them, selenate (SeO_4^{2-}) and selenite (SeO_3^{2-}) are the most bioavailable and are particularly prone to adsorption onto metal oxides, natural organic matter (NOM), and clay minerals (Supriatin et al. 2015). These interactions influence the environmental distribution, redox transformations, mobility, and overall bioavailability of Se. Rapid transformation between particulate and soluble forms further enhances Se's mobility in soil (Tolu et al. 2014).

Selenite (SeO_3^{2-}), in particular, can adsorb onto metal oxide surfaces or form inner-sphere complexes with NOM. These interactions can either enhance or reduce Se bioavailability, depending on the specific mechanisms involved (Dinh et al. 2017). Therefore, understanding the roles of NOM and iron minerals in Se dynamics is critical.

Iron (hydro)oxides, particularly those with high adsorption capacities such as magnetite, lepidocrocite (Lep), hematite, and goethite, play a key role in immobilizing Se(IV) through various mechanisms including complexation, chelation, and direct adsorption (Francisco et al. 2018; Rovira et al. 2008). Lep is a common, poorly crystalline, and metastable iron mineral found in environments undergoing seasonal redox fluctuations. These dynamic redox conditions significantly impact iron mineral transformations (Qin et al. 2023). Lep is characterized by high specific surface area and notable surface reactivity. According to Das et al. (2013), Se(VI) adsorption on Lep occurs predominantly on inner surfaces. However, Lep rarely exists in isolation; it typically coexists with NOM, which can further influence Se adsorption and transport in natural environments (Bao et al. 2022).

Humic acids (HA) account for approximately 55% to 90% of dissolved organic carbon in both aquatic and terrestrial environments (Bogusz et al. 2024; Olaetxea et al. 2018; Zhang et al. 2020). HA can influence the speciation and spatial distribution of Se by forming stable complexes (Qin et al. 2012). In complex geochemical systems, Se retention and distribution are governed by interactions with natural organic matter (NOM), which ultimately affects its mobility, reactivity, and bioavailability. Se can also adsorb directly onto NOM-metal complexes, such as those formed with Fe or Al, resulting in ternary Se-NOM-metal complexes. The high abundance of functional groups in HA, along with its ability to chelate metal ions, plays a central role in these interactions (Weng et al. 2011). Research on Se adsorption has primarily focused on individual effects of iron (hydro)oxide nanoparticles or HA. However, studies have largely overlooked the complex, nanoscale interactions that occur in heterogeneous soil ecosystem where these components coexist.

Terashima et al. (2023) reported that iron-induced binding between Selenium and humic substances can preferentially occur under groundwater conditions. Likewise, Fan et al. (2019) investigated the influence of HA on iron redox transformations in submerged soils and its effect on Se bioavailability. They observed that HA reduces Se bioavailability in wetlands and paddy soils by limiting the release of both Se and Fe into the soil solutions. Despite the frequent co-existence of NOM (particularly HA) and relatively stable iron (hydro)oxide nanoparticles such as Lep, few studies have directly examined how HA-Lep interactions influence Se speciation, distribution, and bioavailability in natural environments.

To mimic conditions prevailing in natural environments, a mixture of synthetic Lep and HA was used with the combination with Se solutions. Focusing on the mechanisms driving Se behavior, this study aims to elucidate the pivotal role of Lep-HA complex microunits in controlling Se speciation and distribution between solid and liquid phases under diverse conditions. Furthermore, various characterization techniques, including SEM and FTIR, are used to investigate the interaction mechanisms among HA, Lep, and Se. This study aims to provide new insights into how HA affects the transformation of iron minerals and, consequently, influences Se speciation.

Materials and methods

Reagents and materials

Ultrapure water ($18.2 \text{ M}\Omega\cdot\text{cm}^{-1}$) was used to prepare the solutions, and all chemicals used in the experiments were of analytical grade. Lep was synthesized following the procedure described by Das et al. (2013). Specifically a solution of FeCl_3 was prepared by dissolving 11.93 g of $\text{FeCl}_2\cdot 4\text{H}_2\text{O}$ in 300 mL of ultrapure water and subsequently oxidized. During the reaction, the pH was maintained within the range of 6.7 to 6.9 by the gradual addition of 120 mL of 1 M NaOH. The resulting precipitate was collected, thoroughly rinsed, and freeze-dried. A stock solution of Lep (300 mg/L) was prepared by dispersing 0.3 g of the freeze-dried Lep in 1 L of ultrapure water. To prepare the HA solution, 5 g of HA (Sigma-Aldrich) was dissolved in 1 L of ultrapure water, and the pH was then adjusted to approximately 11 using 0.1 M KOH. Elemental analysis was conducted of HA, conducted using an elemental

analyzer (Elementar Vario Macro), yielded the following composition: 41.98% C, 3.19% H, 54.39% O, and 0.44% S. The total organic carbon (TOC) concentration of the HA solution was determined to be approximately 2,234 mg C/L using a TOC analyzer (Elementar Vario), and the solution was stored for future use. Prior to use, NaCl was added to adjust the ionic strength to 10 mM. Sodium selenite (0.1095g) was dissolved in a 500 mL volumetric flask to make a 100 mg/L stock solution, which was stored at -4°C for future use.

Impact of pH and HA concentration on Se adsorption by Lep

Batch experiments simulating natural environmental conditions were conducted to investigate the adsorption of Se onto Lep. Equal volumes (49.5 mL each) of Lep (300 mg/L) and HA (80 mg C/L) were mixed and pre-equilibrated in 100 mL glass bottles for 12 hours at 25°C . Two additional treatment groups were prepared: one by mixing 49.5 mL of water with 49.5 mL of Lep (300 mg/L), and the other by mixing 49.5 mL of water with 49.5 mL of HA (80 mg C/L), ensuring consistent volumes and homogeneity across all experimental conditions. Following the pre-equilibrium period, 1 mL of Se solution (4 mg/L) was added to the mixture, and the pH was adjusted to 6. This resulted in final concentrations of 150 mg/L for Lep, 40 mg C/L for HA, and 40 $\mu\text{g/L}$ for Se in each suspension. Samples were collected at predefined intervals (15, 30, 60, 240, 480, and 1440 min), sequentially filtered, and analyzed to determine the distribution of Se across different size fractions.

To study the impact of varying pH levels on Se speciation transformation in Lep-HA-Se suspensions, the pH was adjusted to 4, 5, 6, 7, and 8 (± 0.1), and the mixtures were shaken for 12 h. To assess the impact of HA concentration on Se adsorption by Lep, 49.5 mL of a 300 mg/L Lep suspension was mixed with 49.5 mL of HA solutions at concentrations of 20, 40, 80, 160, and 200 mg C/L, yielding final HA concentrations of 10, 20, 40, 80, and 100 mg C/L. These mixtures were then equilibrated under oscillation for 12 h. Subsequently, 1 mL of Se solution (4 mg/L) was added to each system, resulting in a final Se concentration of 40 $\mu\text{g/L}$, and the pH was adjusted to 6. The mixtures underwent oscillatory equilibration again for 12 h. Se concentrations were measured using hydride generation atomic fluorescence spectrometry (HG AFS-9700). After filtration through a 450 nm membrane, the Zeta potential and kinetic diameter of the colloidal and solution fractions from the different HA concentration treatment groups were measured using dynamic light scattering (DLS). This approach supports the elucidation of Se distribution in the Lep-HA-Se system at the nanoscale. Se was categorized into three size fractions: particulate ($>450 \text{ nm}$), colloidal (3–450 nm), and dissolved ($<10 \text{ kDa}$). To ensure the accuracy and consistency of the results, all experiments were conducted in triplicate.

Characterization

The prepared HA, Lep, HA-Se, Lep-Se, and Lep-HA-Se samples were collected following freeze-drying. To investigate their chemical structure, particularly functional group composition, the potassium bromide (KBr) pellet method was utilized. Fourier-transform infrared spectroscopy (FTIR, Thermo Nicolet 6700, USA) was used to perform the analysis. Spectra were recorded in the range of 400 to 4000 cm^{-1} to capture

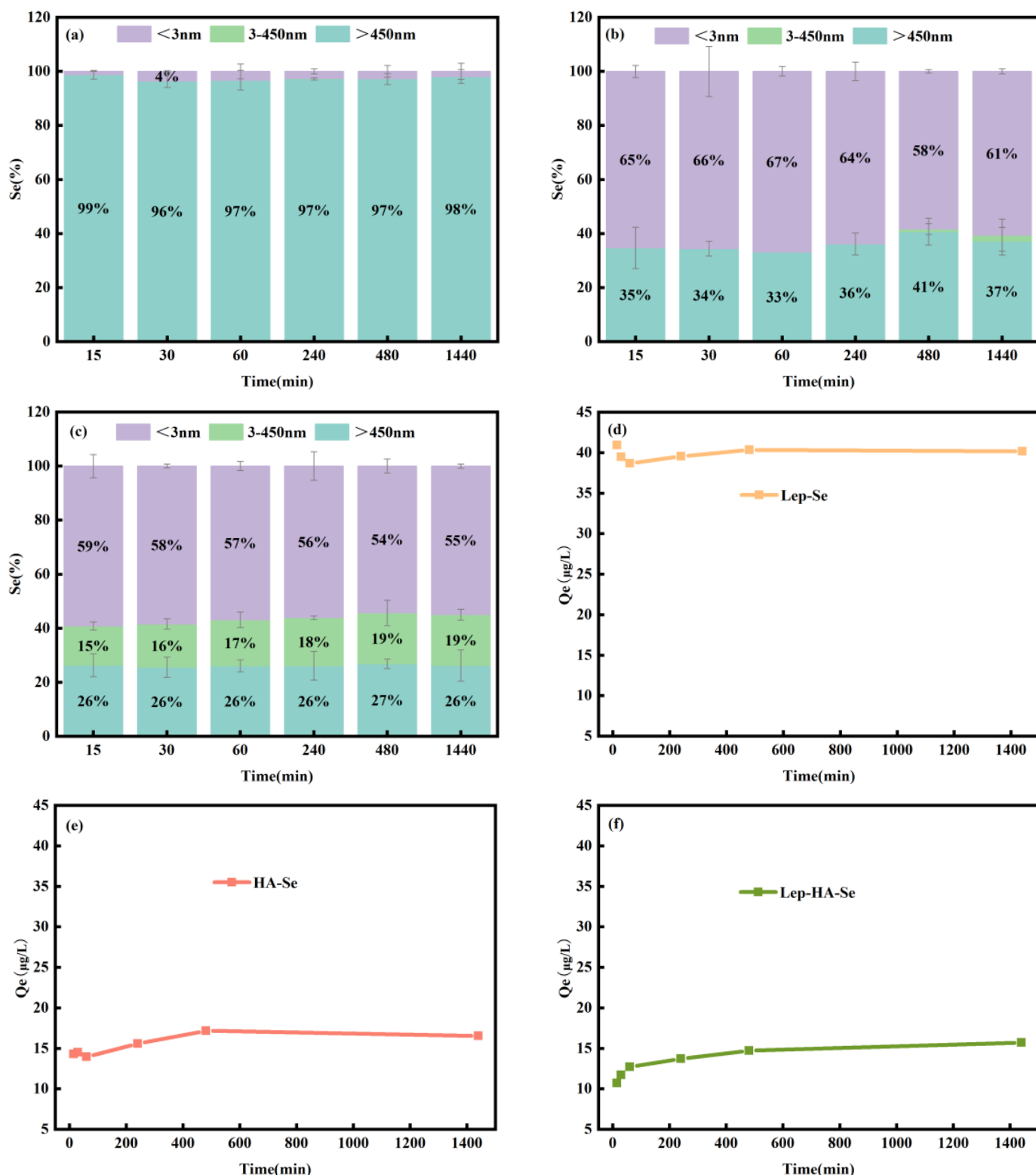


Fig. 1. Percentage of Se concentrations in (a) Lep-Se, (b) HA-Se, and (c) Lep-HA-Se suspension in the size fractions as a function of time. Variation in Se Adsorption Capacity on (d) Lep and (e) HA, and (f) Lep-HA system; (Experiment condition: pH 6 ± 0.5 ; 10 mM NaCl; 40 mg C/L HA; 150 mg/L Lep; 40 µg/L Se). The percentages represent the proportion of Se in each form relative to the total Se, and the error bars indicate the range of error based.

a wide array of chemical bond vibrations, with a resolution of 4 cm^{-1} to ensure high data accuracy. Each spectrum was averaged over 32 scans to improve the signal-to-noise ratio and enhance data reliability. To observe changes in the solid morphology of the Lep, Lep-Se, Lep-HA, and Lep-HA-Se after reaction, freeze-dried samples were examined using scanning electron

microscopy (SEM, EM 30, Korea) operated at an accelerating voltage of 20 kV. The high-resolution imaging capability of SEM provided in-depth insights into microstructure, particle shape, and possible aggregation or dispersion of the samples, thereby revealing physical transformations resulting from the reaction.

Results and discussion

HA influences the distribution of Se in the HA and Lep-HA system

Se adsorbed on Lep occurs rapidly, reaching equilibrium within 15 min in the absence of HA. Due to the strong binding affinity between Se and Lep, over 98% of Se was adsorbed onto Lep under these conditions, with the equilibrium adsorption capacity (Q_e , representing Se adsorbed on particles >450 nm) reaching 40 $\mu\text{g/L}$ (Fig. 1a and d). This process is driven primarily by electrostatic interactions between the positively charged surfaces of Lep and the negatively charged Se anions. Additionally, the relatively high specific surface area of Lep provides abundant active sites for Se adsorption (Das et al. 2013). Most of the adsorbed Se was associated with the particulate fraction, consistent with the particulate nature of Lep (Fig. 1a). Similarly, Se was rapidly

absorbed onto HA, with approximately 37% of Se associated with the particulate fraction and about 60% remaining in the dissolved phase within 15 minutes, corresponding to a Q_e of about 17 $\mu\text{g/L}$. The presence of HA significantly influenced Se speciation and distribution, promoting the formation of dissolved Se species (Fig. 1c and f). In the Lep-Se mixture, the particulate Se fraction ranged from 96.7 to 98.7%, compared to 33.1 to 40.7% in the HA-Se mixture, and 25.6 to 26.8% in the Lep-HA-Se mixture. Conversely, dissolved Se fraction was only 1.3 to 3.6% in the Lep-Se system but increased to 58.4 to 66.9% in the HA-Se system, and to 54.4 to 59.2% in the Lep-HA-Se system. In the Lep-HA-Se mixture, Se was also present in the colloidal form, ranging from 14.5 to 18.8%. Over time, concentrations of both dissolved and colloidal Se increased.

The Q_e of Se in the Lep-HA mixture was notably lower (~ 14 $\mu\text{g/L}$) than in systems containing either Lep or HA alone,

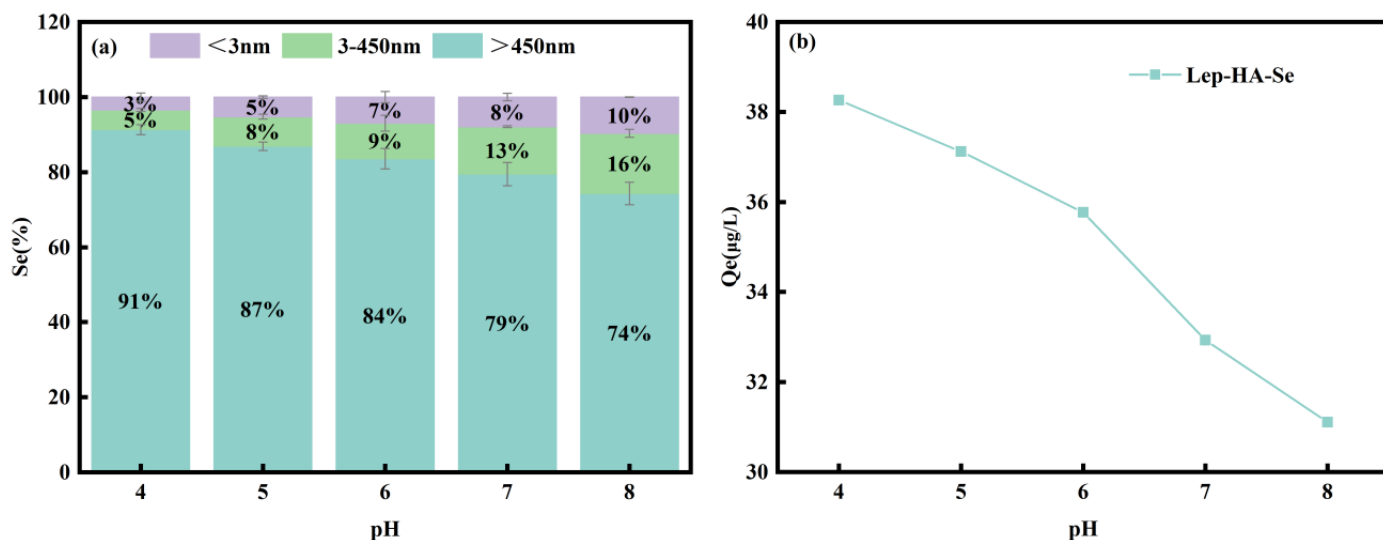


Fig. 2. (a) Effect of pH on Se adsorption by the Lep-HA System, (b) Variation in Se Adsorption Capacity by Lep under different pH conditions. (10 mM NaCl; 40 mg C/L HA; 150 mg/L Lep; 40 $\mu\text{g/L}$ Se. The percentages represent the proportion of Se in each form relative to the total Se, and the error bars indicate the range of error from three replicate experiments).

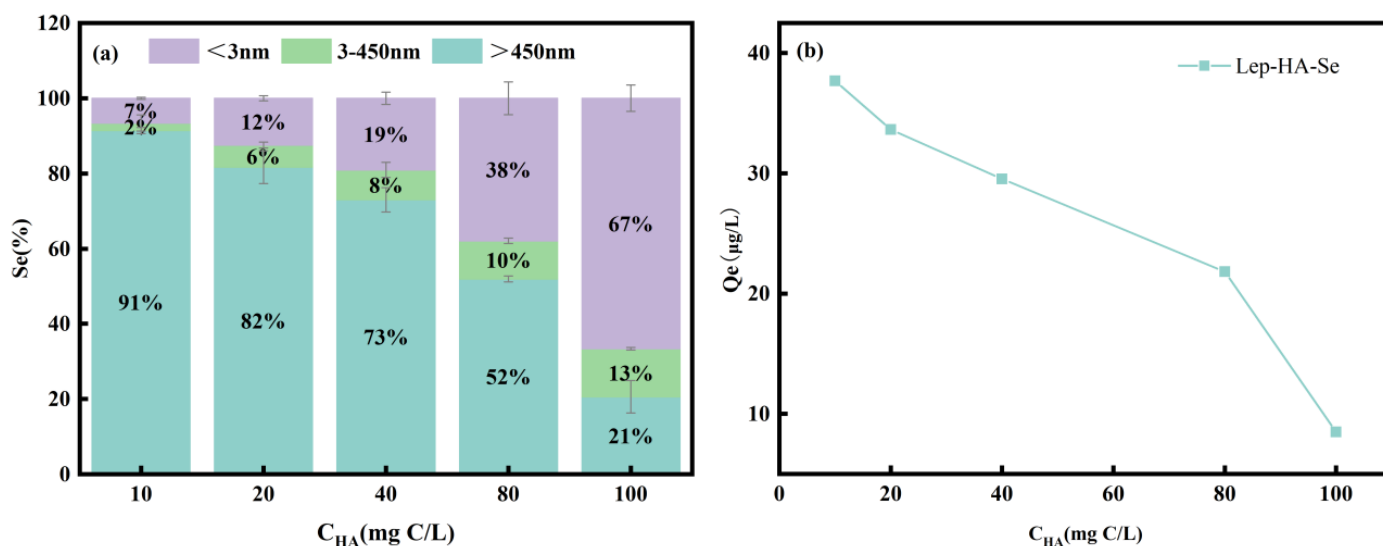


Fig. 3. (a) Effect of HA concentration on the distribution of Se species adsorbed by Lep, (b) Variation in Se Adsorption Capacity by Lep under Different HA Concentrations. (Experimenting condition: pH 6 ± 0.5 ; 10 mM NaCl; 150 mg/L Lep; 40 $\mu\text{g/L}$ Se. The percentages represent the proportion of Se in each form relative to the total Se, and the error bars indicate the range of error from three replicate experiments).

suggesting that HA influenced the redistribution and speciation of Se. This may be attributed to the ability of NOM to form aqueous and surface-bound complexes with cationic metals and metal oxides. Interaction between HA and Lep likely modified the surface characteristics of Lep, reducing the number of available adsorption sites. Furthermore, the adsorption process is influenced by surface site availability, charge interactions, and rate of complexation between dissolved Se species and the surface sites (Bu et al. 2023; Pintor et al. 2020). Compared to other minerals, iron oxides like Lep generally offer a greater number of binding sites (Peng et al. 2022). However, the substantial reduction in Se adsorption in the Lep-HA system may be due to HA occupying a significant portion of the adsorption sites. Organic ligands in HA can chelate surface sites, thereby hindering Se diffusion to the oxide surface and reducing its adsorption, resulting in elevated concentrations of dissolved and colloidal Se (Bu et al. 2023; Favorito et al. 2018).

Effect of pH on Se adsorption by Lep-HA complex

The pH influences not only the surface charge of Lep but also its complexation behavior with HA. As pH changes the degree of HA protonation, HA competes with Lep for Se adsorption sites, thereby influencing Se adsorption efficiency (Kusmierk et al. 2023). As shown in Fig. 2a, the concentrations of dissolved and colloidal Se increase with rising pH, consistent with the findings of Favorito et al. (2018). Specifically, as the pH increased from 4 to 8, the proportions of dissolved Se rose from approximately 3.4% to 9.7%, colloidal Se from 5.7% to 16.0%, while particulate Se decreased from 91.3% to 74.3%, indicating a substantial reduction in solid-phase adsorption. This trend is consistent with the known behavior of metal oxides in SeO_3^{2-} adsorption, where increasing pH typically reduces adsorption capacity within environmentally relevant pH ranges (Francisco et al. 2018). At higher pH levels, HA becomes increasingly deprotonated, resulting in a more negatively charged structure. This intensifies electrostatic repulsion both among HA molecules and between HA and SeO_3^{2-} , while also diminishing

the attractive forces between Se and the Lep surface (Fig. 4b), thereby limiting Se adsorption (Cheng et al. 2024; Sefalhi et al. 2024). At lower pH values, H^+ ions preferentially adsorb onto Lep surfaces, enhancing their positive charge and strengthening electrostatic attraction with negatively charged Se species. Conversely, increasing pH leads to the ionization of acidic functional groups, enhancing electrostatic repulsion. This not only weakens Se adsorption but also inhibits aggregation of Se particulates, further reducing overall adsorption capacity (Alsaiairi et al. 2024; Xie et al. 2017).

Effect of HA concentrations on Se Adsorption by Lep

As illustrated in Fig. 3a and b, an increase in HA concentration was accompanied by a decrease in Se adsorption by Lep. The proportions of dissolved and colloidal Se increased in parallel with rising HA concentrations. At 100 mg C/L HA, particulate Se accounted for only 20%. This phenomenon can be attributed to the strong interactions between the functional groups of HA and the surface of Lep, resulting in competition between HA and Se for available adsorption sites. As the HA concentration increased from 10 to 100 mg C/L, a greater number of adsorption sites on the Lep surface were occupied by HA. This led to a notable decrease in Se adsorption and a corresponding increase in the concentration of unbound Se (Xie et al. 2017).

To further investigate the impact of HA concentration on Se distribution, particle size and Zeta potential were measured across various HA concentrations (Fig. 4). Under conditions of constant pH, uniform ionic strength, and consistent HA chemical composition, the interaction between Lep and HA is primarily governed by the molecular size and structural characteristics of HA (Terashima et al. 2023). In the presence of HA concentrations ranging from 10 to 100 mg/L, Lep-HA complexes exhibited a hydrodynamic diameter of approximately 130 nm, indicating the formation of relatively stable colloidal structures. This stability is attributed to the ability of HA to stabilize iron particles within the colloidal size range at higher concentrations (Xing et al. 2020). When Se was introduced, the hydrodynamic diameters of Lep-HA-Se increased to 90.81,

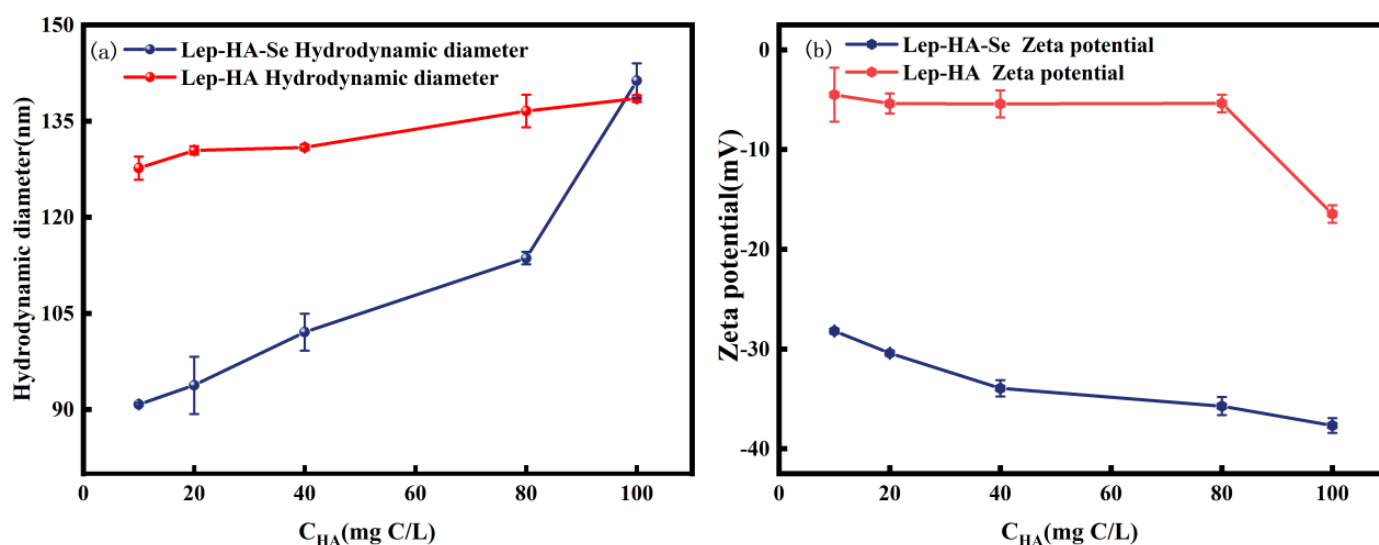


Fig 4. The impact of varying HA concentrations on particle size and Zeta potential. (a) The hydrodynamic diameter for Lep-HA-Se and Lep-HA; (b) The Zeta potential for Lep-HA-Se and Lep-HA. (Samples were filtered through a 450 nm membrane to assess the particle size distribution of the dissolved and colloidal phases; $\text{pH}6 \pm 0.5$; 10 mM NaCl; 150 mg/L Lep; 40 $\mu\text{g/L}$ Se. Error bars represent the range from three replicate experiments).

93.77, 102.07, 113.62, and 141.29 nm, respectively (Fig. 4a), suggesting variation in particle size distribution due to the incorporation of Se. These results confirm that the increase in particle size is associated with the presence of Se colloids. Se adsorption onto Lep-HA was also found to reduce the surface charge, leading to particle aggregation. Conversely, increasing organic matter content enhanced the negative surface charge and improved colloidal stability (Xing et al. 2020).

A decrease in Zeta potential was observed in the presence of the reactive solute SeO_3^{2-} , attributed to its adsorption onto iron oxide surfaces (Fig. 4b). The variation in surface charge of Lep-HA at low and high HA concentrations is hypothesized to be linked to surface coverage. At 100 mg/L C, particles are likely fully coated with HA, masking the electrochemical properties of the underlying iron oxide surfaces (Siéliéchi et al. 2008). Additionally, the presence of Se was shown to potentially reduce HA adsorption due to competitive ion effect. At higher HA concentrations, Se may exhibit increased mobility. This behavior is likely due to the coating of iron hydroxide surfaces by organic matter and the propensity of soluble organic acids to form complexes with Se, thereby affecting its stability and mobility (Dinh et al. 2017). As a result, concentrations of dissolved and colloidal selenium species increased. Because SeO_3^{2-} is an anionic species, it is expected to influence adsorption processes similarly HA, chiefly by reducing surface charge, attracting cations, and promoting the formation of ternary surface complexes.

Characterization analysis

FTIR spectroscopy was utilized to analyze changes in HA functional groups to investigate how HA impacted Se adsorption onto Lep (Fig. 5). HA is a complex NOM exhibiting characteristic peaks corresponding to various

functional groups. The broad peak observed at 3200-3500 cm^{-1} is attributed to O-H stretching vibrations (from carboxyl and hydroxyl groups), while peaks in the range of 2800-3000 cm^{-1} correspond to C-H stretching vibrations (aliphatic and aromatic groups). An intense peak in the range of 1600-1700 cm^{-1} is ascribed to C=O stretching vibrations (carboxyl and carbonyl groups), and peaks in the range of 1400-1500 cm^{-1} are likely associated with C-H bending or symmetric stretching of carboxylate groups (Park et al. 2011). These functional groups suggest that HA has abundant surface-active sites capable of interacting with Lep and Se via hydrogen bonding, coordination, or electrostatic forces. Lep, a typical iron oxyhydroxide, displayed a distinct broad peak in the FTIR spectra within the range of 3200-3600 cm^{-1} , attributed to the O-H stretching vibration of Fe-O-H. This indicates that the Lep surface is rich in -OH groups, which serve as primary active sites for interactions with HA and Se. Additionally, peaks observed in the range of 1000-1200 cm^{-1} may correspond to vibrations of Fe-O bonds (Rahimi et al. 2021). These characteristic peaks confirm that the Lep surface possesses numerous active sites capable of forming interactions with HA and Se through coordination or hydrogen bonding.

Compared to Lep, the FTIR spectra of the Lep-HA complex exhibited a noticeable shift in the O-H peak within the range of 3200-3600 cm^{-1} , indicating hydrogen bonding interactions between the hydroxyl groups of HA and the Fe-O-H groups on the Lep surface. Additionally, the reduced intensity of the C=O peak in the range of 1600-1700 cm^{-1} suggests that the carboxyl groups of HA may coordinate with the iron sites on the Lep surface (Yuan et al. 2023; Zhang et al. 2021). These results demonstrate that HA interacts strongly with the Lep surface through its abundant functional groups, potentially

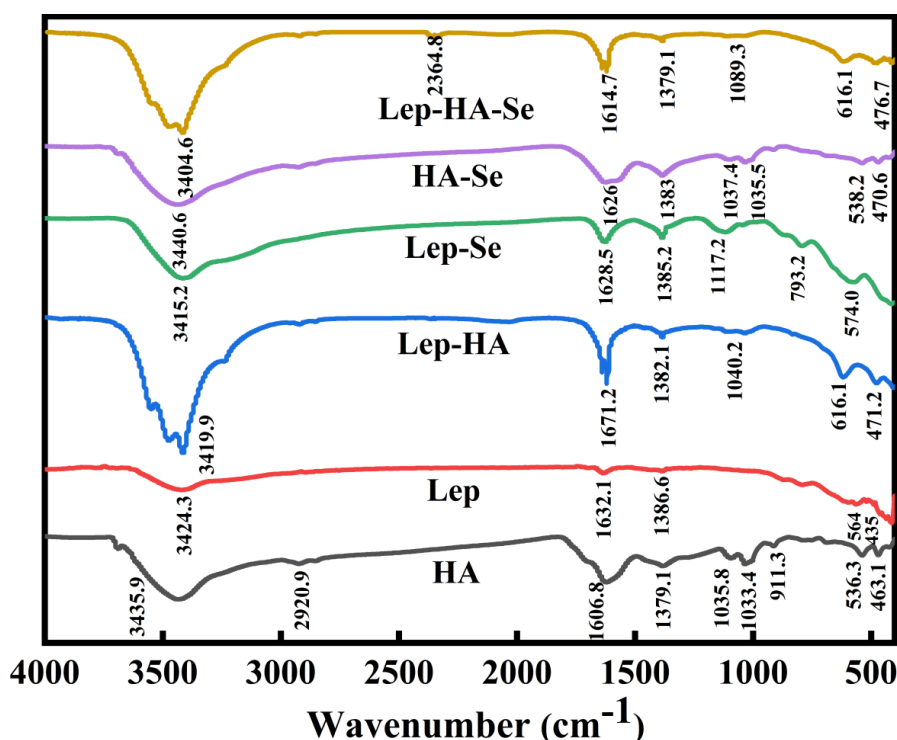


Fig. 5 FTIR analysis of Lep, HA, Lep-HA, Lep-Se, HA-Se, and Lep-HA-Se. (pH6 ± 0.5; 10 mM NaCl; 40 mg C/L HA; 150 mg/L Lep; 40 µg/L Se).

influencing the adsorption capacity for Se. The spectra of the Lep-Se complex reveal slight shifts in both the Fe-O-H ($3200\text{--}3600\text{ cm}^{-1}$) and Fe-O ($1000\text{--}1200\text{ cm}^{-1}$) peaks, indicating that Se is adsorbed onto the hydroxyl groups and iron sites on the Lep surface. This observation aligns with the inner-sphere coordination mechanism of Se on iron oxide surfaces reported in previous studies (Kumpulainen et al. 2008). Se may adsorb onto the Lep surface by displacing hydroxyl groups or forming coordination bonds with iron. In the spectra of the Lep-HA-Se complex, significant changes are observed in the O-H peak ($3200\text{--}3600\text{ cm}^{-1}$) and the C=O peak ($1600\text{--}1700\text{ cm}^{-1}$) (Jia et al. 2013). The shift in the O-H peak suggests competitive adsorption among Se, HA, and Lep hydroxyl groups, while

the decreased C=O peak intensity indicates that HA's carboxyl groups may participate in Se coordination. Furthermore, the shift in the Fe-O peak ($1000\text{--}1200\text{ cm}^{-1}$) confirms the interaction between Se and the iron sites on the Lep surface (Peng et al. 2022). These results suggest that HA significantly modifies Lep's adsorption characteristics for Se, potentially through competitive or synergistic effects.

Based on the comprehensive analysis of FTIR spectra, the mechanisms by which HA influences Se adsorption onto Lep can be summarized as follows: (1) Competitive adsorption: the hydroxyl and carboxyl groups of HA strongly interact with hydroxyl groups and iron sites on the Lep surface, potentially occupying adsorption sites and competing with Se for binding.

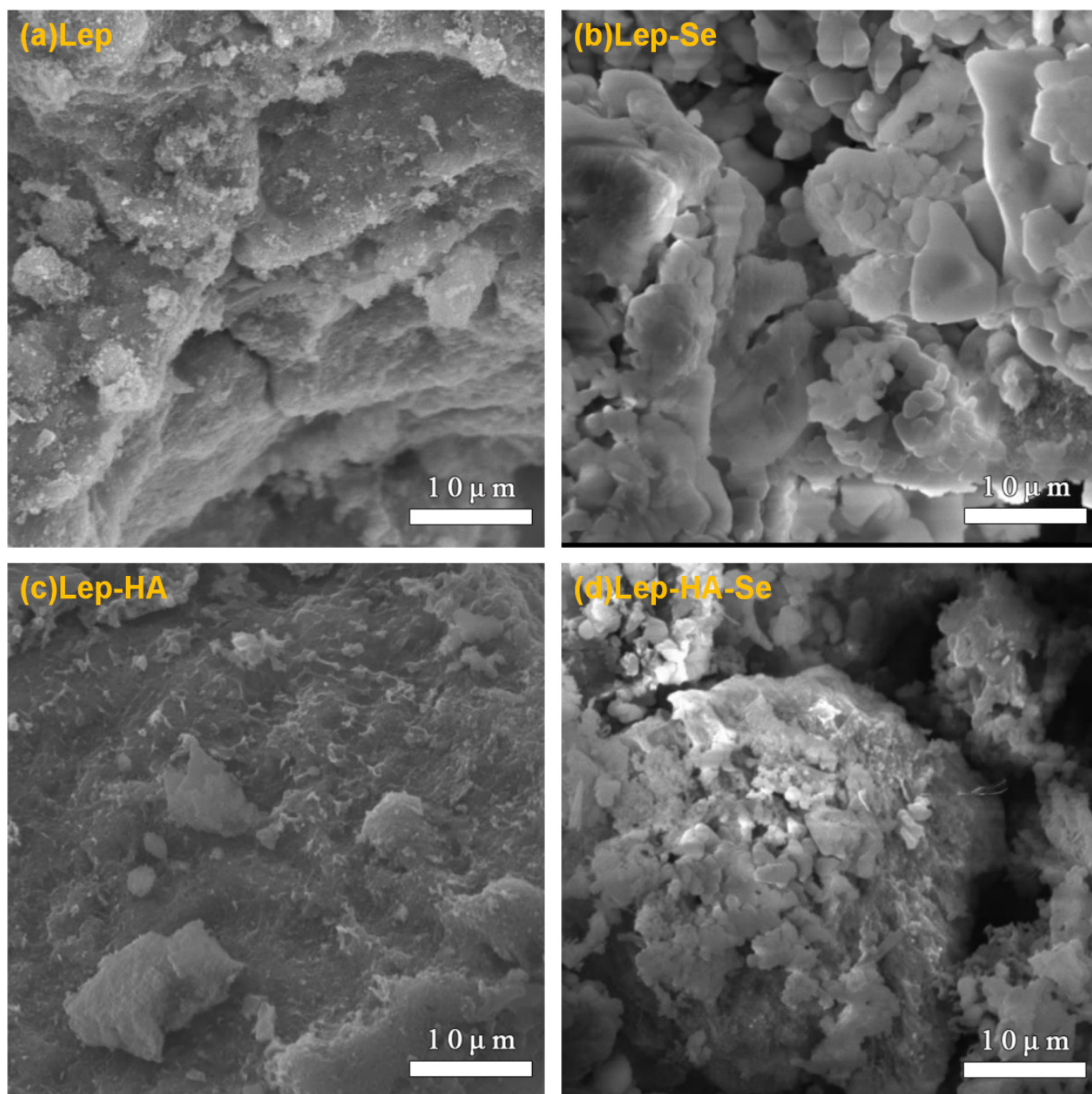


Fig. 6 SEM analysis of (a) Lep, (b) Lep-Se, (c) Lep-HA, and Lep-HA-Se. (pH 6 ± 0.5 ; 10 mM NaCl; 40 mg C/L HA; 150 mg/L Lep; 40 $\mu\text{g/L}$ Se)

(2) Coordination: carboxyl groups of HA may form coordination bonds with Se, altering its adsorption morphology and stability. (3) Surface modification: HA adsorption on the Lep surface may modify its surface charge and hydrophobicity, thereby affecting Se adsorption behavior. These results demonstrate that HA plays a complex and significant role in modulating Se adsorption on Lep through multiple interaction pathways.

SEM imaging provided a visual representation of the initial surface morphology of Lep, revealing stacked, rough, and irregular flakes (Fig. 6). The observed morphology is consistent with the plate-like and blocky structure previously described by Das et al. (2013). Following Se adsorption, notable morphological changes were observed. The initially dense and compact structure became more relaxed, with individual particles more clearly distinguishable. These changes likely result from interactions between Lep and Se, leading to surface modification and the possible formation of Se-containing complexes (Yoon et al. 2011). Further alterations were evident upon the co-adsorption of HA and Se. The surface exhibited increased aggregation and cluster formation, resulting in a more heterogeneous and less uniform morphology compared to Lep-Se. This transformation is likely due to the deposition of HA coatings, which introduce additional complexity and contribute to the irregular and bulky appearance. These HA layers may influence both the adsorption behavior and chemical reactivity of the Lep particles (Bu et al. 2023).

Mechanisms of HA affected Se adsorption on Lep

The mechanisms by which HA influences Se adsorption on Lep are multifaceted, involving competitive adsorption, coordination interactions, and surface modification. HA competes with Se for adsorption sites on the Lep surface through its abundant functional groups, such as -OH and -COOH groups. This competition is evidenced by shifts in the O-H (3200-3600 cm^{-1}) and C=O (1600-1700 cm^{-1}) peaks in the FTIR spectra, indicating hydrogen bonding and coordination between HA and Lep surface sites. Additionally, the carboxyl groups of HA can form coordination bonds with Se, thereby altering its adsorption morphology and stability. Surface modification by HA further reduces Se adsorption by altering Lep's surface charge and hydrophobicity, as demonstrated by changes in Zeta potential and hydrodynamic diameter. At higher HA concentrations, increased electrostatic repulsion and colloidal stabilization enhance the mobility of dissolved and colloidal Se, leading to reduced particulate Se adsorption. pH also plays a critical role: lower pH levels favor Se adsorption due to surface protonation effects, while higher pH conditions promote Se mobility. Collectively, these mechanisms highlight HA's significant role in modulating Se adsorption behavior, emphasizing its impact on Se speciation, distribution, and environmental mobility in systems involving iron oxides and NOM.

Conclusion

This study elucidates the complex mechanisms by which HA influences the adsorption of Se onto Lep, highlighting the pivotal role of HA in regulating Se speciation, distribution, and mobility within environmental systems. The findings reveal that HA significantly alters Se adsorption behavior through three primary mechanisms: competitive adsorption, coordination

interactions, and surface modification. Specifically, HA competes with Se for adsorption sites on the Lep surface via its functional groups, such as hydroxyl and carboxyl groups, as evidenced by shifts in FTIR spectra. Additionally, HA forms coordination bonds with Se, altering its adsorption morphology and stability. Surface modification induced by HA further reduces Se adsorption by changing Lep's surface charge and hydrophobicity, as supported by Zeta potential and hydrodynamic diameter analyses. At higher HA concentrations, increased electrostatic repulsion and colloidal stabilization enhance the mobility of dissolved and colloidal Se, consequently reducing its particulate fraction. Moreover, pH emerges as a critical factor; lower pH conditions favor Se adsorption through surface protonation, whereas higher pH levels enhance Se desorption and mobility. Collectively, these results underscore the significant role of HA in controlling Se bioavailability and mobility in natural environments, particularly in geochemical systems where iron oxides and NOM coexist.

This study provides valuable insights into the geochemical cycling of Se and offers practical guidance for managing Se-rich agricultural systems to optimize Se bioavailability while mitigating associated environmental risks. Moving forward, future research should prioritize investigating these interactions under dynamic redox conditions to better simulate field environments. Additionally, employing advanced spectroscopic and molecular techniques will be essential for uncovering the precise binding mechanisms at the molecular scale. From an applied standpoint, developing HA-based strategies to optimize Se bioavailability in agricultural systems, alongside comprehensive assessment of the environmental risks posed by colloidal Se-HA transport in groundwater, represent critical areas for further exploration. Such multidisciplinary efforts will not only improve predictive models of Se behavior but also inform more effective management practices in both Se-deficient and Se-contaminated ecosystems.

Declaration of Competing Interest

The authors declare that they have no known competing financial interests or personal relationships that could have appeared to influence the work reported in this paper.

Acknowledgments

This research has been supported by the National Natural Science Foundation of China (NO. 42267030).

Reference:

- Alsaiani, R., Shedaiwa, I., Al-Qadri, F.A., Musa, E.M., Alqahtani, H., Alkorbi, F., Alsaiani, N.A. & Mohamed, M.M. (2024). Peganum Harmala L. plant as green non-toxic adsorbent for iron removal from water. *Archives of Environmental Protection*, 50,1, pp. 3-12. DOI:10.24425/aep.2024.149427.
- Bao, Y., Bolan, N.S., Lai, J., Wang, Y., Jin, X., Kirkham, M.B., Wu, X., Fang, Z., Zhang, Y. & Wang, H. (2022). Interactions between organic matter and Fe (hydr)oxides and their influences on immobilization and remobilization of metal(loid)s: A review. *Critical Reviews in Environmental Science and Technology*, 52, 22, pp. 4016-4037. DOI:10.1080/10643389.2021.1974766.

- Bogusz, P., Zimnoch, U., Brodowska, M.S. & Michalak, J. (2024). The trend of changes in soil organic carbon content in Poland over recent years. *Archives of Environmental Protection*, 50,1, pp. 35-44. DOI:10.24425/aep.2024.149430.
- Bu, H., Lei, Q., Tong, H., Liu, C., Hu, S., Xu, W., Wang, Y., Chen, M. & Qiao, J. (2023). Humic acid controls cadmium stabilization during Fe(II)-induced lepidocrocite transformation. *Science of the Total Environment*, 861, pp. 160624. DOI:10.1016/j.scitotenv.2022.160624.
- Cheng, B., Liu, J., Li, X., Yue, L., Cao, X., Li, J., Wang, C. & Wang, Z. (2024). Bioavailability of selenium nanoparticles in soil and plant: the role of particle size. *Environmental and Experimental Botany*, 220, pp. 105682. DOI:10.1016/j.envexpbot.2024.105682.
- Das, S., Jim Hendry, M. & Essilfie-Dughan, J. (2013). Adsorption of selenate onto ferrihydrite, goethite, and lepidocrocite under neutral pH conditions. *Applied Geochemistry*, 28, pp. 185-193. DOI:10.1016/j.apgeochem.2012.10.026.
- Dinh, Q.T., Li, Z., Tran, T.A.T., Wang, D. & Liang, D. (2017). Role of organic acids on the bioavailability of selenium in soil: A review. *Chemosphere*, 184, pp. 618-635. DOI:10.1016/j.chemosphere.2017.06.034.
- Fan, J., Zhao, G., Sun, J., Hu, Y. & Wang, T. (2019). Effect of humic acid on Se and Fe transformations in soil during waterlogged incubation. *Science of the Total Environment*, 684, pp. 476-485. DOI:10.1016/j.scitotenv.2019.05.246.
- Favorito, J.E., Eick, M.J. & Grossl, P.R. (2018). Adsorption of Selenite and Selenate on Ferrihydrite in the Presence and Absence of Dissolved Organic Carbon. *Journal of Environmental Quality*, 47,1, pp. 147-155. DOI:10.2134/jeq2017.09.0352.
- Francisco, P.C.M., Sato, T., Otake, T., Kasama, T., Suzuki, S., Shiwaku, H. & Yaita, T. (2018). Mechanisms of Se(IV) Co-precipitation with Ferrihydrite at Acidic and Alkaline Conditions and Its Behavior during Aging. *Environmental Science & Technology*, 52, 8, pp. 4817-4826. DOI:10.1021/acs.est.8b00462.
- Jia, Y., Luo, T., Yu, X.-Y., Sun, B., Liu, J.-H. & Huang, X.-J. (2013). Synthesis of monodispersed α -FeOOH nanorods with a high content of surface hydroxyl groups and enhanced ion-exchange properties towards As(v). *RSC Advances*, 3, 36, pp. 15805-15811. DOI:10.1039/C3RA40980E.
- Kumpulainen, S., von der Kammer, F., Hofmann, T. (2008). Humic acid adsorption and surface charge effects on schwertmannite and goethite in acid sulphate waters. *Water Research*, 42,8, pp. 2051-2060. DOI: 10.1016/j.watres.2007.12.015.
- Kusmieriek, K., Dabek, L. & Swiatkowski, A. (2023). Removal of Direct Orange 26 azo dye from water using natural carbonaceous materials. *Archives of Environmental Protection*, 49,1, pp. 47-56. DOI:10.24425/aep.2023.144736.
- Li, Z., Liang, D., Peng, Q., Cui, Z., Huang, J. & Lin, Z. (2017). Interaction between selenium and soil organic matter and its impact on soil selenium bioavailability: A review. *Geoderma*, 295, pp. 69-79. DOI:10.1016/j.geoderma.2017.02.019.
- Olaetxea, M., De Hita, D., Garcia, C.A., Fuentes, M., Baigorri, R., Mora, V., Garnica, M., Urrutia, O., Erro, J., Zamarreño, A.M., Berbara, R.L. & Garcia-Mina, J.M. (2018). Hypothetical framework integrating the main mechanisms involved in the promoting action of rhizospheric humic substances on plant root- and shoot- growth. *Applied Soil Ecology*, 123, pp. 521-537. DOI:10.1016/j.apsoil.2017.06.007.
- Park, J.H., Lamb, D., Paneerselvam, P., Choppala, G., Bolan, N. & Chung, J.-W. (2011). Role of organic amendments on enhanced bioremediation of heavy metal(loid) contaminated soils. *Journal of Hazardous Materials*, 185,2, pp. 549-574. DOI:10.1016/j.jhazmat.2010.09.082.
- Peng, J., Fu, F., Ye, C. & Tang, B. (2022). Interaction between Se(IV) and fulvic acid and its impact on Se(IV) immobility in ferrihydrite-Se(IV) coprecipitates during aging. *Environmental Pollution*, 293, pp. 118552. DOI:10.1016/j.envpol.2021.118552.
- Pintor, A.M.A., Vieira, B.R.C., Brandão, C.C., Boaventura, R.A.R. & Botelho, C.M.S. (2020). Complexation mechanisms in arsenic and phosphorus adsorption onto iron-coated cork granulates. *Journal of Environmental Chemical Engineering*, 8, 5, pp. 104184. DOI:10.1016/j.jece.2020.104184.
- Qin, H.-B., Zhu, J.-M. & Su, H. (2012). Selenium fractions in organic matter from Se-rich soils and weathered stone coal in selenosis areas of China. *Chemosphere*, 86, 6, pp. 626-633. DOI:10.1016/j.chemosphere.2011.10.055.
- Qin, L., Wang, M., Sun, X., Yu, L., Wang, J., Han, Y. & Chen, S. (2023). Formation of ferrihydrite induced by low pe+pH in paddy soil reduces Cd uptake by rice: Evidence from Cd isotope fractionation. *Environmental Pollution*, 328, pp. 121644. DOI:10.1016/j.envpol.2023.121644.
- Rahimi, S., Soleimani, M. & Azadmehr, A.R. (2021). Performance Evaluation of Synthetic Goethite and Lepidocrocite Nanoadsorbents for the Removal of Aniline from a Model Liquid Fuel through Kinetic and Equilibrium Studies. *Energy & Fuels*, 35, 13, pp. 10659-10668. DOI:10.1021/acs.energyfuels.1c00474.
- Ros, G.H., van Rotterdam, A.M.D., Bussink, D.W. & Bindraban, P.S. (2016). Selenium fertilization strategies for bio-fortification of food: an agro-ecosystem approach. *Plant and Soil*, 404, 1, pp. 99-112. DOI:10.1007/s11104-016-2830-4.
- Rovira, M., Giménez, J., Martínez, M., Martínez-Lladó, X., de Pablo, J., Martí, V. & Duro, L. (2008). Sorption of selenium(IV) and selenium(VI) onto natural iron oxides: Goethite and hematite. *Journal of Hazardous Materials*, 150, 2, pp. 279-284. DOI:10.1016/j.jhazmat.2007.04.098.
- Sefatli, K.L., Ultra, V.U., Stephen, M., Oleszek, S. & Manyiwa, T. (2024). Adsorption of nitrate and phosphate ions using ZnCl₂-activated biochars from phytoremediation biomasses. *Archives of Environmental Protection*, 50, 3, pp. 65-83. DOI:10.24425/aep.2024.151687.
- Siéliéchi, J.M., Lartiges, B.S., Kayem, G.J., Hupont, S., Frochot, C., Thieme, J., Ghanbaja, J., d'Espinose de la Caillerie, J.B., Barrès, O., Kamga, R., Levitz, P. & Michot, L.J. (2008). Changes in humic acid conformation during coagulation with ferric chloride: Implications for drinking water treatment. *Water Research*, 42, 8, pp. 2111-2123. DOI:10.1016/j.watres.2007.11.017.
- Supriatin, S., Weng, L. & Comans, R.N.J. (2015). Selenium speciation and extractability in Dutch agricultural soils. *Science of the Total Environment*, 532, pp. 368-382. DOI:10.1016/j.scitotenv.2015.06.005.
- Terashima, M., Endo, T., Kimuro, S., Beppu, H., Nemoto, K. & Amano, Y. (2023). Iron-induced association between selenium and humic substances in groundwater from deep sedimentary formations. *Journal of Nuclear Science and Technology*, 60, 4, pp. 374-384. DOI:10.1080/00223131.2022.2111376.
- Tolu, J., Thiry, Y., Bueno, M., Jolivet, C., Potin-Gautier, M. & Le Hécho, I. (2014). Distribution and speciation of ambient selenium in contrasted soils, from mineral to organic rich. *Science of the Total Environment*, 479-480, pp. 93-101. DOI:10.1016/j.scitotenv.2014.01.079.

- Weng, L., Vega, F.A., Supriatin, S., Bussink, W. & Riemsdijk, W.H.V. (2011). Speciation of Se and DOC in Soil Solution and Their Relation to Se Bioavailability. *Environmental Science, Technology*, 45,1, pp. 262-267. DOI:10.1021/es1016119.
- Xie, Y., Dong, H., Zeng, G., Zhang, L., Cheng, Y., Hou, K., Jiang, Z., Zhang, C. & Deng, J. (2017). The comparison of Se(IV) and Se(VI) sequestration by nanoscale zero-valent iron in aqueous solutions: The roles of solution chemistry. *Journal of Hazardous Materials*, 338, pp. 306-312. DOI:10.1016/j.jhazmat.2017.05.053.
- Xing, B., Ouyang, M., Graham, N. & Yu, W. (2020). Enhancement of phosphate adsorption during mineral transformation of natural siderite induced by humic acid: Mechanism and application. *Chemical Engineering Journal*, 393, pp. 124730. DOI:10.1016/j.cej.2020.124730.
- Ying, H. & Zhang, Y. (2019). Systems Biology of Selenium and Complex Disease. *Biological Trace Element Research*, 192, 1, pp. 38-50. DOI:10.1007/s12011-019-01781-9.
- Yoon, I.-H., Kim, K.-W., Bang, S. & Kim, M.G. (2011). Reduction and adsorption mechanisms of selenate by zero-valent iron and related iron corrosion. *Applied Catalysis B: Environmental*, 104,1, pp. 185-192. DOI:10.1016/j.apcatb.2011.02.014.
- Yuan, Z., Su, R., Ma, X., Yu, L., Pan, Y., Chen, N., Chernikov, R., Cheung, L.K.L., Deevsalar, R., Tunc, A., Wang, L., Zeng, X., Lin, J. & Jia, Y. (2023). Direct immobilization of Se(IV) from acidic Se(IV)-rich wastewater via ferric selenite Coprecipitation. *Journal of Hazardous Materials*, 460, pp. 132346. DOI:10.1016/j.jhazmat.2023.132346.
- Zhang, H., Xie, S., Bao, Z., Tian, H., Carranza, E.J.M., Xiang, W., Yao, L. & Zhang, H. (2020). Underlying dynamics and effects of humic acid on selenium and cadmium uptake in rice seedlings. *Journal of Soils and Sediments*, 20, 1, pp. 109-121. DOI:10.1007/s11368-019-02413-4.
- Zhang, J., Wang, X., Zhan, S., Li, H., Ma, C. & Qiu, Z. (2021). Synthesis of Mg/Al-LDH nanoflakes decorated magnetic mesoporous MCM-41 and its application in humic acid adsorption. *Microchemical Journal*, 162, pp. 105839. DOI:10.1016/j.microc.2020.105839.